Available online at www.sciencedirect.com
ScienceDirect
International Journal of Solids and Structures 44 (2007) 6987–6998
INTERNATIONAL JOURNAL OF SOLIDS AND STRUCTURES
www.elsevier.com/locate/ijsolstr

Strain energy density of a circular cavity buried in a semi-infinite slab of functionally graded materials subjected to anti-plane shear waves

Xue-Qian Fang [a,*], Chao Hu [a,b], Wen-Hu Huang [a]

[a] Department of Aerospace Engineering and Mechanics, Harbin Institute of Technology, P.O. Box137, Harbin 150001, China
[b] School of Aerospace Engineering and Applied Mechanics, Tongji University, Shanghai 200092, China

Received 17 December 2006; received in revised form 12 March 2007
Available online 30 March 2007

Abstract

The paper presents a theoretical method to investigate the multiple scattering of shear waves and strain energy density in a semi-infinite slab of functionally graded materials with a circular cavity. The analytical solutions of wave fields are expressed by employing wave function expansion method and the expanded mode coefficients are determined by satisfying the boundary conditions of the cavity. Image method is used to satisfy the free boundary condition of the semi-infinite structure. The analytical solution of the problem is derived, and the numerical solutions of the strain energy density factors around the cavity are also graphically presented. The effects of the distances between the cavity and the boundaries of the semi-infinite slab, the wave number and the non-homogeneous parameter of materials on strain energy density factors are analyzed. Analyses show that the strain energy density around the cavity increases with increasing non-homogeneous parameter of materials and incident wave number. The boundaries of the semi-infinite slab have great effect on both the maximum strain energy density and the distribution around the circular cavity, and the effect increases with increasing incident wave number. When the distance between the semi-infinite boundary and the cavity varies, the effect of the upper and lower boundaries on the distribution of the strain energy density factors around the cavity is also examined.

Keywords: Semi-infinite slabs; Exponentially graded materials; Multiple scattering of elastic waves; Strain energy density factor; Circular cavity

1. Introduction

Functionally graded materials (FGMs) are a new generation of engineering materials wherein the microstructural details are spatially varied through non-uniform distributions of the reinforcement phases, by using reinforcements with different properties, sizes and shapes, as well as by interchanging the roles of reinforcement and matrix phases in a continuous manner (Aboudi et al., 1999). For example, ceramics are useful in

* Corresponding author. Tel.: +86 451 86410268; fax: +86 451 89264194.
E-mail address: fangxueqian@163.com (X.-Q. Fang).

0020-7683/$ - see front matter © 2007 Elsevier Ltd. All rights reserved.
doi:10.1016/j.ijsolstr.2007.03.024

high strength and temperature applications. However, they suffer from low toughness. In an ideal FGM, they may be combined in an intelligent manner with a metal of high toughness to raise the toughness of the combination.

To meet the requirements of engineering design, it is inevitable to make cutouts in functionally graded material structures, and some failures such as cavities and cracks may also occur during the serving of the structures. Under dynamic loads, the stress and potential energy density around and near the discontinuities may increase sharply, which causes the growth of cavities or cracks and decrease the strength of the structures. The theoretical analysis and experimental investigations of this problem have received considerable attention over past several decades.

At present, most literatures focus on employing the numerical method to solve the dynamic stress and strain energy density around and near the discontinuities in composite materials. These numerical methods include finite element method (Roussseau and Tippur, 2001; Tan and Meguid, 1996), boundary element method (Rice and Sadd, 1984; Sladek et al., 2005) and Laplace and Fourier integral transforms technique (Li and Weng, 2000; Ueda, 2001). For the dynamic stress in FGMs, Roussseau and Tippur (2001) applied finite element method to analyze the effect of different elastic gradient profiles on the fracture behavior of dynamically loaded functionally graded materials having cracks parallel to the elastic gradient. A meshless local boundary element method was used to study the dynamic anti-plane shear crack problem in functionally graded materials (Sladek et al., 2005). Laplace and Fourier integral transforms and a numerical Laplace inversion technique were also used to analyze the dynamic stress intensity factor of cracks in functionally graded materials under impact load (Li and Weng, 2000; Ueda, 2001). Recently, the dynamic problem of a Yoffe crack in an infinite strip of FGMs subjected to anti-plane shear loading was studied, and the strain energy density factor at the crack tip was obtained by using integral transforms and dual-integral equations (Bi et al., 2003).

Although these numerical methods are very useful tools for these problems, it is also very important to determine the physical behavior of the problems with analytical method. Pao and Chao (1964) investigated the multiple scattering of elastic waves and dynamic stress concentration in a thin plate with cutouts, and the analytical and numerical solutions of the problem were presented. The scattering of flexural waves produced by a row of circular inclusions in plate was studied by Klyukin (1964), and the analytical solution was presented. Recently, image method was applied to analyze the elastic wave scattering and dynamic stress concentrations in the plate having a circular cavity subjected to plane harmonic SH waves (Hayir and Bakirtas, 2004). Most recently, Fang et al. (2006) employed wave function expansion method and image method to study the multiple scattering and strain energy density of a circular cavity buried in semi-infinite functionally graded materials subjected to shear waves.

It is well known that many practical engineering structures have boundaries, and are not ideally infinite. However, because the boundaries of structures reflect the elastic waves and vibration, complex problems such as the multiple scattering of elastic waves may arise. In this field, very few literatures were reported in the past (Fang et al., 2006). The main objective of this paper is to investigate the multiple scattering of elastic waves and strain energy density factor (SEDF) in a semi-infinite slab of functionally graded materials with a circular cavity. The S-theory (Sih, 1973) is applied to determine the crack initiation and direction for the cavity in the semi-infinite slab of functionally graded materials. This fracture criterion makes use of a parameter called strain energy density factor which is a function of the stress intensity factors. The strain energy density theory provides a more general treatment of fracture mechanics problems by virtue of its ability in describing the multi-scale feature of material damage and in dealing with mixed mode crack propagation problem (Nobile et al., 2004). The wave fields are expanded by employing the wave functions expansion method, and the expanded mode coefficients are determined by satisfying the boundary condition of the cavity. Image method is used to satisfy the boundary condition of traction free surfaces. The analytical solution of strain energy density factor is presented. The effects of the geometric and material parameters on the strain energy density factors around the cavity are also analyzed.

2. Wave motion equation and its solution

A semi-infinite slab of functionally graded materials is considered, as depicted in Fig. 1. A circular cavity with radius a is embedded in the slab, the distances between the center of the cavity and the boundaries of the

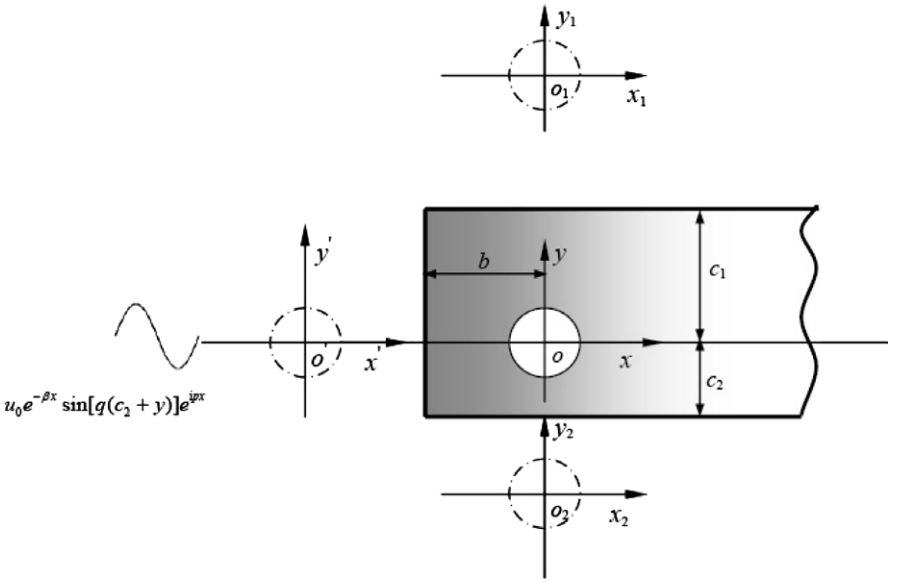

Fig. 1. Schematic of a semi-infinite slab of functionally graded materials with a circular cavity.

semi-infinite slab are denoted as b, c_1 and c_2. An anti-plane shear wave with frequency ω is incident on the surface in the positive x direction.

For simplicity, it is assumed that the shear modulus and density of materials vary continuously in the $x$direction, the variations of them are proposed as

$$\mu(x) = \mu_0 \exp(2\beta x), \quad \rho(x) = \rho_0 \exp(2\beta x), \tag{1}$$

where μ_0 and ρ_0 are the shear modulus and density of materials at the position of $x = 0$, respectively, and β is a non-homogeneous parameter which denotes the exponent of spatial variation of the shear modulus and density of materials (Kuo and Chen, 2005). Though the variations are unrealistic, it would allow us to comprehend the effect of material gradient on the characteristic of wave propagation.

The anti-plane governing equation in materials is described as

$$\frac{\partial \tau_{xz}}{\partial x} + \frac{\partial \tau_{yz}}{\partial y} = \rho \frac{\partial^2 u}{\partial t^2}, \tag{2}$$

where τ_{xz} and τ_{yz} are the anti-plane shear stresses, and u is the displacement field.

The constitutive relations of anti-plane shear displacement are

$$\tau_{xz} = \mu(x)\frac{\partial u}{\partial x}, \quad \tau_{yz} = \mu(x)\frac{\partial u}{\partial y}. \tag{3}$$

Substitution of Eq. (3) into Eq. (2) yields the following equation

$$\frac{\partial^2 u}{\partial x^2} + \frac{\partial^2 u}{\partial y^2} + 2\beta\frac{\partial u}{\partial x} = \frac{1}{c_s^2}\frac{\partial^2 u}{\partial t^2}, \tag{4}$$

where $c_s = \sqrt{\mu_0/\rho_0}$ is the wave speed of shear waves.

The steady solution of this problem is investigated. Let $u = U\exp(-i\omega t)$, Eq. (4) can be changed into the following equation

$$\nabla^2 U + 2\beta\frac{\partial U}{\partial x} + k^2 U = 0, \tag{5}$$

where ω is the circular frequency of the incident waves, and $k = \omega/c_s$ is the wave number of elastic waves.

The form of the solution of Eq. (5) can be proposed as

$$U = \exp(-\beta x) w(x, y), \tag{6}$$

where $w(x,y)$ is the function introduced for derivation.

Substituting Eq. (6) into Eq. (5), one can see that the function $w(x,y)$ should satisfy the following question

$$\nabla^2 w + \kappa^2 w = 0, \tag{7}$$

where $\kappa = \sqrt{k^2 - \beta^2}$.

According to Eqs. (5)–(7), it can be seen that there exist elastic waves with the form of $U e^{-i\omega t} = u_0 \exp(-\beta x) e^{i(\kappa x - \omega t)}$, which denotes the propagating wave with its amplitude of vibration attenuating in the x direction.

In order to apply the complex variable method, the complex variables $z = x + iy$ and $\bar{z} = x - iy$ are introduced. Then Eq. (7) can be transformed into the equation about the variables of z and $\bar{z}$

$$\frac{\partial^2 w}{\partial z \partial \bar{z}} + \left(\frac{\kappa}{2}\right)^2 w = 0. \tag{8}$$

The general solution of the scattered field resulting from the circular cavity in FGMs is expressed as

$$u = \exp(-\beta r \cos\theta) \sum_{n=-\infty}^{\infty} A_n H_n^{(1)}(\kappa r) e^{in\theta} = \exp(-\beta \mathrm{Re}\, z) \sum_{n=-\infty}^{\infty} A_n H_n^{(1)}(\kappa |z|) \left\{\frac{z}{|z|}\right\}^n. \tag{9}$$

where $H_n^{(1)}(\cdot)$ is the nth Hankel function of the first kind, A_n determined by satisfying the boundary condition are the mode coefficients of the scattered waves, and $\mathrm{Re}(z)$ denotes the real part of complex variable z.

3. The excitation of elastic waves and the total wave field

Consider an anti-plane shear wave propagating along the positive x direction. Based on the constructive interference theory of wave fields, the wave field in the semi-infinite slab of functionally graded materials can be described as

$$u = f(y) \exp(-\beta x) \exp[i(px - \omega t)]. \tag{10}$$

The solution of Eq. (10) should satisfy Eq. (4), and then the following expression can be obtained

$$f(y) = A\cos(qy) + B\sin(qy), \tag{11}$$

where p and q are the longitudinal and transversal wave numbers, respectively, and $p^2 = \kappa^2 - q^2 = k^2 - \beta^2 - q^2$.

Suppose that the upper and lower boundaries are free of traction. Thus, function $f(y)$ should satisfy the following equation

$$f(c_1)\mu(x) = 0, \quad f(-c_2)\mu(x) = 0. \tag{12}$$

So, the transversal wave number is expressed as

$$q = \frac{n\pi}{c_1 + c_2} \quad (n = 0, 1, 2, \ldots, \infty). \tag{13}$$

Substitution of Eq. (13) into (10) yields the expression of displacement in functionally graded materials

$$u = B\sin[q(c_2 + y)] \exp(-\beta x) \exp[i(px - \omega t)]. \tag{14}$$

The reflected waves are described by employing the image method. Note that the $n = 1$ mode is investigated in this paper.

If the upper and lower boundaries are free of traction, the incident wave field can be proposed as

$$u^{(\mathrm{i})} = u_0 \exp(-\beta x)\sin[q(c_2+y)]\mathrm{e}^{\mathrm{i}[p(x+b)-\omega t]} = u_0 \sin[q(c_2+y)]\mathrm{e}^{-\beta x+\mathrm{i}pb}\sum_{n=-\infty}^{\infty}\mathrm{i}^n J_n(pr)\mathrm{e}^{\mathrm{i}n\theta}\mathrm{e}^{-\mathrm{i}\omega t}, \tag{15}$$

where u_0 is the displacement amplitude of the incident waves, p is the wave number in the x direction, and $J_n(\cdot)$ is the nth Bessel function.

Considering the multiple scattering at the boundaries of $y = c_1$ and $y = -c_2 (c_1 > 0,\ c_2 > 0)$, the scattered field resulting from the circular cavity can be described, in the polar coordinate system, as

$$u^{(\mathrm{s})} = \exp(-\beta x)\left\{\sum_{n=-\infty}^{\infty} A_n H_n^{(1)}(\kappa r)\mathrm{e}^{\mathrm{i}n\theta} + \sum_{n=-\infty}^{\infty} A_n(-1)^n H_n^{(1)}(\kappa r')\mathrm{e}^{-\mathrm{i}n\theta'} + \sum_{m=1}^{\infty}\left[\sum_{n=-\infty}^{\infty} A_n H_n^{(1)}(\kappa r_m)\mathrm{e}^{\mathrm{i}n\theta_m} + \sum_{n=-\infty}^{\infty} A_n(-1)^n H_n^{(1)}(\kappa r'_m)\mathrm{e}^{-\mathrm{i}n\theta'_m}\right]\right\}. \tag{16}$$

It should be noted that m denotes the series index representing the image cavities.

For simplicity, the scattered field is expressed in the form of complex variables

$$u^{(\mathrm{s})} = \exp[-\beta \mathrm{Re}(z)]\left\{\sum_{n=-\infty}^{\infty} A_n H_n^{(1)}(\kappa|z|)\left\{\frac{z}{|z|}\right\}^n + \sum_{n=-\infty}^{\infty} A_n(-1)^n H_n^{(1)}(\kappa|z-z_0|)\left\{\frac{z-z_0}{|z-z_0|}\right\}^n + \sum_{n=-\infty}^{\infty} A_n \sum_{m=1}^{\infty}\sum_{l=1}^{4}\left[H_n^{(1)}(\kappa|z-z_{lm}|)\left\{\frac{z-z_{lm}}{|z-z_{lm}|}\right\}^n\right] + \sum_{n=-\infty}^{\infty} A_n \sum_{m=1}^{\infty}\sum_{l=1}^{4}\left[(-1)^n H_n^{(1)}(\kappa|z-z_0-z_{lm}|)\left\{\frac{z-z_0-z_{lm}}{|z-z_0-z_{lm}|}\right\}^n\right]\right\}, \tag{17}$$

where $z_0 = -2b,\ z_{1m} = 2\mathrm{i}(mL - c_2),\ z_{2m} = \mathrm{i}2mL,\ z_{3m} = -2\mathrm{i}[(m-1)L + c_2],\ z_{4m} = -2\mathrm{i}mL,\ L = c_1 + c_2,$ and $m = 1,2,\ldots,\infty$.

The total wave field in materials is taken to be a superposition of the incident waves and the scattered waves, i.e.

$$u^{(\mathrm{t})} = u^{(\mathrm{i})} + u^{(\mathrm{s})}. \tag{18}$$

4. Determination of mode coefficients and strain energy density factor

Without loss of generality, the case that the boundary condition is free of traction is investigated. The boundary condition is that the radial shear stress is equal to zero, i.e.

$$\tau_{rz}|_{r=a} = \mu(r,\theta)\left.\frac{\partial u}{\partial r}\right|_{r=a} = 0. \tag{19}$$

Substitution of Eq. (18) into Eq. (19) yields the following equations

$$\sum_{n=-\infty}^{+\infty} E_n X_n = E, \tag{20}$$

where

$$
\begin{aligned}
E_n = & -\beta \mathrm{Re}\left(\frac{z}{|z|}\right)\exp[-\beta \mathrm{Re}(z)]\left\{H_n^{(1)}(\kappa|z|)\left\{\frac{z}{|z|}\right\}^n + (-1)^n H_n^{(1)}(\kappa|z-z_0|)\left\{\frac{z-z_0}{|z-z_0|}\right\}^n\right. \\
& \left. + \sum_{m=1}^{\infty}\sum_{l=1}^{4}\left[H_n^{(1)}(\kappa|z-z_{lm}|)\left\{\frac{z-z_{lm}}{|z-z_{lm}|}\right\}^n\right] + \sum_{m=1}^{\infty}\sum_{l=1}^{4}\left[(-1)^n H_n^{(1)}(\kappa|z-z_0-z_{lm}|)\left\{\frac{z-z_0-z_{lm}}{|z-z_0-z_{lm}|}\right\}^n\right]\right\} \\
& + \exp[-\beta \mathrm{Re}(z)]\left\{\frac{1}{2}\kappa[H_{n-1}^{(1)}(\kappa|z|) - H_{n+1}^{(1)}(\kappa|z|)]\left\{\frac{z}{|z|}\right\}^n\right. \\
& + \frac{1}{2}\kappa(-1)^n\frac{1}{|z|}|z-z_0|\mathrm{Re}\left\{\frac{z}{z-z_0}\right\}[H_{n-1}^{(1)}(\kappa|z-z_0|) - H_{n+1}^{(1)}(\kappa|z-z_0|)]\left\{\frac{z-z_0}{|z-z_0|}\right\}^n \\
& + \mathrm{i}n(-1)^n\frac{1}{|z|}\mathrm{Im}\left\{\frac{z}{z-z_0}\right\}H_n^{(1)}(\kappa|z-z_0|)\left\{\frac{z-z_0}{|z-z_0|}\right\}^n \\
& + \frac{1}{2}\sum_{m=1}^{\infty}\sum_{l=1}^{4}\kappa\frac{1}{|z|}|z-z_{lm}|\mathrm{Re}\left\{\frac{z}{z-z_{lm}}\right\}[H_{n-1}^{(1)}(\kappa|z-z_{lm}|) - H_{n+1}^{(1)}(\kappa|z-z_{lm}|)]\left\{\frac{z-z_{lm}}{|z-z_{lm}|}\right\}^n \\
& + \sum_{m=1}^{\infty}\sum_{l=1}^{4}\mathrm{i}n\frac{1}{|z|}\left\{\frac{z-z_{lm}}{|z-z_{lm}|}\right\}^n\mathrm{Im}\left\{\frac{z}{z-z_{lm}}\right\}H_n^{(1)}(\kappa|z-z_{lm}|)\left\{\frac{z-z_{lm}}{|z-z_{lm}|}\right\}^n \\
& + \frac{1}{2}\sum_{m=1}^{\infty}\sum_{l=1}^{4}(-1)^n\kappa\frac{1}{|z|}|z-z_0-z_{lm}|\mathrm{Re}\left\{\frac{z}{z-z_0-z_{lm}}\right\}[H_{n-1}^{(1)}(\kappa|z-z_0-z_{lm}|) \\
& - H_{n+1}^{(1)}(\kappa|z-z_0-z_{lm}|)]\left\{\frac{z-z_0-z_{lm}}{|z-z_0-z_{lm}|}\right\}^n \\
& \left. + \sum_{m=1}^{\infty}\sum_{l=1}^{4}(-1)^n\ \mathrm{i}n\frac{1}{|z|}\mathrm{Im}\left\{\frac{z}{z-z_0-z_{lm}}\right\}H_n^{(1)}(\kappa|z-z_0-z_{lm}|)\left\{\frac{z-z_0-z_{lm}}{|z-z_0-z_{lm}|}\right\}^n\right\}, \qquad (21)
\end{aligned}
$$

$$
\begin{aligned}
E = & -u_0\mathrm{e}^{-\beta x}\,\mathrm{e}^{\mathrm{i}p(x+b)}\{\beta\cos\theta\sin[q(c_2+y)] \\
& + \{q\sin\theta\cos[q(c_2+y)] + \mathrm{i}p\cos\theta\sin[q(c_2+y)]\}\} \\
= & -u_0\mathrm{e}^{-\beta x+\mathrm{i}pb}\{-\beta\cos\theta\sin[q(c_2+y)] + \{q\sin\theta\cos[q(c_2+y)] \\
& + \mathrm{i}p\cos\theta\sin[q(c_2+y)]\}\}\sum_{n=-\infty}^{\infty}\mathrm{i}^n J_n(pr)\mathrm{e}^{\mathrm{i}n\theta}, \qquad (22)
\end{aligned}
$$

and $X_n = A_n$.

Multiplying by $\mathrm{e}^{-\mathrm{i}s\theta}$ at both sides of Eq. (20), and then integrating from $-\pi$ to π, the following expressions can be obtained

$$\sum_{n=-\infty}^{+\infty} E_{ns}X_n = E_s \quad (n = s = 0, \pm1, \pm2, \ldots), \qquad (23)$$

Here the elements of matrix are determined by the following equations

$$E_{ns} = \frac{1}{2\pi}\int_{-\pi}^{\pi} E_n\mathrm{e}^{-\mathrm{i}s\theta}\,\mathrm{d}\theta, \quad E_s = \frac{1}{2\pi}\int_{-\pi}^{\pi} E\mathrm{e}^{-\mathrm{i}s\theta}\,\mathrm{d}\theta. \qquad (24)$$

Note that Eq. (23) are the infinite algebra equation systems determining all mode coefficients A_n. By making use of the orthogonality relations of $\mathrm{e}^{-\mathrm{i}s\theta}$, one obtains, for each $n \geqslant 0$, a set of algebraic equation system. After arrangement, the equations can be simplified as

$$[E]\{X\} = \{f\}, \qquad (25)$$

where E is a coefficient matrix of $n \times n$, and f is a vector of n ranks.

To obtain the dynamic stress intensity factor, the dynamic stress concentration factor is calculated first. According to the definition of the dynamic stress concentration factor α_{III}, the dynamic stress concentration

factor is the ratio of the hoop shear stress around the cavity and the maximum stress (Pao and Mow, 1973). Thus, the expression of α_{III} around the circular cavity in FGMs is written as

$$\alpha_{\mathrm{III}} = |\tau_{\theta z}/\tau_0|, \tag{26}$$

Here $\tau_{\theta z} = \mu(r,\theta)\dfrac{1}{r}\dfrac{\partial u}{\partial \theta}$

$$\begin{aligned}
&= -\beta\mu(z,\bar{z})\exp[-\beta\,\mathrm{Re}(z)]\left\{\sum_{n=-\infty}^{\infty} A_n H_n^{(1)}(\kappa|z|)\left\{\frac{z}{|z|}\right\}^n\right.\\
&+\sum_{n=-\infty}^{\infty} A_n(-1)^n H_n^{(1)}(\kappa|z-z_0|)\left\{\frac{z-z_0}{|z-z_0|}\right\}^n + \sum_{n=-\infty}^{\infty} A_n \sum_{m=1}^{\infty}\sum_{l=1}^{4} H_n^{(1)}(\kappa|z-z_{lm}|)\left\{\frac{z-z_{lm}}{|z-z_{lm}|}\right\}^n\\
&\left.+\sum_{n=-\infty}^{\infty} A_n \sum_{m=1}^{\infty}\sum_{l=1}^{4}(-1)^n H_n^{(1)}(\kappa|z-z_0-z_{lm}|)\left\{\frac{z-z_0-z_{lm}}{|z-z_0-z_{lm}|}\right\}^n\right\}\\
&+\frac{1}{\mathrm{Re}(z)}\exp[-\beta\mathrm{Re}(z)]\left\{\frac{1}{2}\kappa\sum_{n=-\infty}^{\infty} A_n[H_{n-1}^{(1)}(\kappa|z|) - H_{n+1}^{(1)}(\kappa|z|)]\left\{\frac{z}{|z|}\right\}^n\right.\\
&-\sum_{n=-\infty}^{\infty}\frac{1}{2}\kappa A_n(-1)^n|z-z_0|\mathrm{Im}\left\{\frac{z}{z-z_0}\right\}[H_{n-1}^{(1)}(\kappa|z-z_0|) - H_{n+1}^{(1)}(\kappa|z-z_0|)]\left\{\frac{z-z_0}{|z-z_0|}\right\}^n\\
&+\sum_{n=-\infty}^{\infty} A_n(-1)^n \mathrm{i}n\mathrm{Re}\left\{\frac{z}{z-z_0}\right\}H_n^{(1)}(\kappa|z-z_0|)\left\{\frac{z-z_0}{|z-z_0|}\right\}^n\\
&-\sum_{n=-\infty}^{\infty}\frac{1}{2}\kappa A_n\sum_{m=1}^{\infty}\sum_{l=1}^{4}|z-z_{lm}|\ \mathrm{Im}\left\{\frac{z}{z-z_{lm}}\right\}[H_{n-1}^{(1)}(\kappa|z-z_{lm}|) - H_{n+1}^{(1)}(\kappa|z-z_{lm}|)]\left\{\frac{z-z_{lm}}{|z-z_{lm}|}\right\}^n\\
&+\sum_{n=-\infty}^{\infty} A_n\sum_{m=1}^{\infty}\sum_{l=1}^{4}\mathrm{i}n\mathrm{Re}\left\{\frac{z}{z-z_0}\right\}H_n^{(1)}(\kappa|z-z_{lm}|)\left\{\frac{z-z_{lm}}{|z-z_{lm}|}\right\}^n\\
&-\frac{1}{2}\kappa\sum_{n=-\infty}^{\infty} A_n\sum_{m=1}^{\infty}\sum_{l=1}^{4}(-1)^n|z-z_0-z_{lm}|\ \mathrm{Im}\left\{\frac{z}{z-z_0-z_{lm}}\right\}[H_{n-1}^{(1)}(\kappa|z-z_0-z_{lm}|)\\
&-H_{n+1}^{(1)}(\kappa|z-z_0-z_{lm}|)]\left\{\frac{z-z_0-z_{lm}}{|z-z_0-z_{lm}|}\right\}^n\\
&+\sum_{n=-\infty}^{\infty} A_n\sum_{m=1}^{\infty}\sum_{l=1}^{4}(-1)^n\mathrm{i}n\mathrm{Re}\left\{\frac{z}{z-z_0-z_{lm}}\right\}H_n^{(1)}(\kappa|z-z_0-z_{lm}|)\left\{\frac{z-z_0-z_{lm}}{|z-z_0-z_{lm}|}\right\}^n\Bigg\}\\
&+u_0\exp[-\beta\,\mathrm{Re}(z)]\mu(z,\bar{z})\{(\beta-\mathrm{i}p)\sin\theta\sin[q(c_2+y)] + q\cos\theta\cos[q(c_2+y)]\}\mathrm{e}^{\mathrm{i}p(x+b)},
\end{aligned} \tag{27}$$

in which τ_0 is the maximum magnitude of the stress resulting from the incident waves, and $\tau_0(r,\theta) = \sqrt{\beta^2+p^2} = \sqrt{(k^2+\pi^2)/L^2}$.

The relation between the dynamic stress intensity factor and the dynamic stress concentration factor is proposed as (Fan, 2003)

$$K_{\mathrm{III}} = \frac{\sqrt{\pi}\tau_0}{2}\alpha_{\mathrm{III}}. \tag{28}$$

According to the theory of strain energy density criterion (Sih, 1973), the minimum strain energy density factor (SEDF) can be expressed as

$$\mathrm{SEDF} = a_{33}K_{\mathrm{III}}^2. \tag{29}$$

where $a_{33} = 1/4\pi\mu(0)$.

Eq. (29) can be normalized by a_{33}, namely,

$$\frac{\mathrm{SEDF}}{\tau_0^2/16\mu(0)} = (\alpha_{\mathrm{III}})^2. \tag{30}$$

5. Numerical examples and discussions

According to the strain energy criterion, the fatigue failures often occur in the regions with high SEDF, so an understanding of the distribution of the SEDFs is very useful in the structural design.

According to the expression of SEDF, the SEDFs around the circular cavity are computed. During the course of computing, it is found that the truncations of $n = 10$ and $m = 12$ in Eqs. (23) and (27) are sufficient to obtain the accurate results at any desired wave number.

In the following analysis, it is convenient to make the variables dimensionless. To accomplish this step, a representative length scale a, where a is the radius of the circular cavity, is introduced. The following dimensionless variables and quantities have been chosen for computation: the incident wave number is $ka = 0.01 - 2.0$, the distance between the center of the cavity and the semi-infinite boundary is $b/a = 1.1 - 5.0$, the distance between the center of the cavity and the upper boundary is $c_1/a = 3.0 - 8.0$, the distance between the center of the cavity and the lower boundary is $c_2/a = 3.0 - 8.0$, and the non-homogeneous parameter is $\beta a = -0.3 - 0.3$.

Fig. 2 displays the angular distribution of the SEDFs around the circular cavity with parameters: $\beta = 0$, $b/a = 1.1$, $c_1/a = 8.0$ and $c_2/a = 8.0$. Note that in this case the upper and lower boundaries have no effect on the SEDFs around the cavity. It can be seen that when the distance is $b/a = 1.1$, because of the multiple scattering between the cavity and the edge of the semi-infinite slab, the SEDFs at the positions near the semi-infinite edge are greater than those at the symmetrical positions about the y axis. The SEDFs around the cavity increase with increasing incident wave number. When the incident wave number is relatively great, the edge of the semi-infinite structure has greater effect on the distribution of the SEDFs around the cavity.

Fig. 3 displays the angular distribution of the SEDFs around the circular cavity with parameters: $\beta = 0$, $b/a = 5.0$, $c_1/a = 8.0$ and $c_2/a = 8.0$. It can be seen that the maximum strain energy density decreases with the increase of the value of b/a, and the angular distribution of SEDFs is approximatively symmetric about both axes. It is also clear that the boundaries of the semi-infinite slab in this case nearly have no effect on the angular distribution of the SEDFs around the cavity. Note that the angular distribution of the SEDFs in this case is consistent with that in previous literature (Fang et al., 2006).

Fig. 4 illustrates the angular distribution of the SEDFs around the circular cavity with parameters: $ka = 0.1$, $b/a = 1.1$, $c_1/a = 8.0$ and $c_2/a = 8.0$. It can be seen that the SEDFs around the cavity increase with increasing non-homogeneous parameter of materials. As the non-homogeneous parameter increases, the effect of the edge of semi-infinite materials increases. The semi-infinite edge makes the position of the maximum strain energy density having a trend of shifting towards the illuminated side of the cavity. The trend of shifting is more evident when the non-homogeneous parameter is greater.

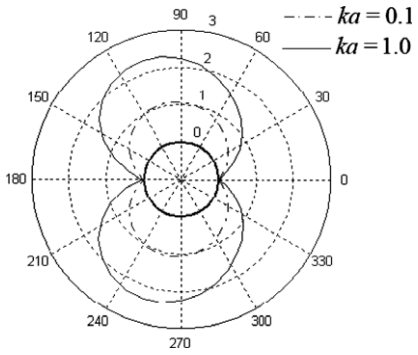

Fig. 2. Angular distribution of normalized strain energy density around the cavity ($\beta = 0$, $b/a = 1.1$, $c_1/a = 8.0$, $c_2/a = 8.0$).

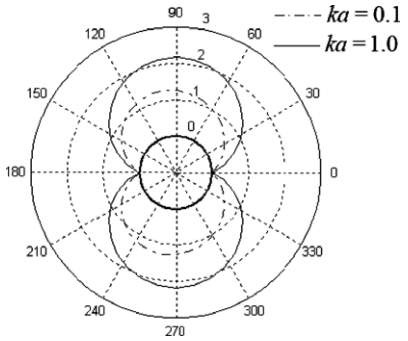

Fig. 3. Angular distribution of normalized strain energy density around the cavity ($\beta = 0$, $b/a = 5.0$, $c_1/a = 8.0$, $c_2/a = 8.0$).

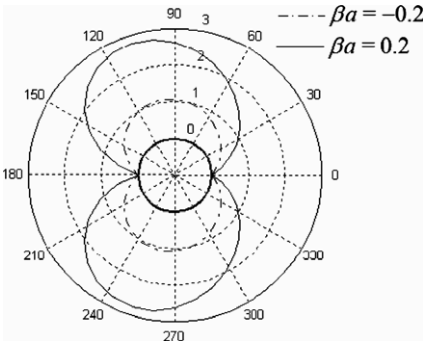

Fig. 4. Angular distribution of normalized strain energy density around the cavity ($ka = 0.5$, $b/a = 1.1$, $c_1/a = 8.0$, $c_2/a = 8.0$).

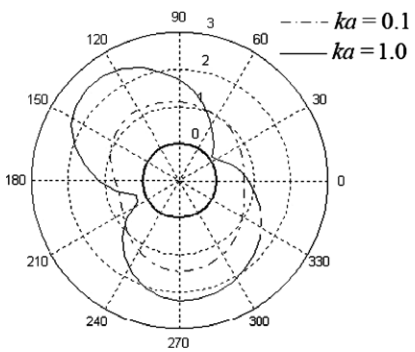

Fig. 5. Angular distribution of normalized strain energy density around the cavity ($\beta a = 0.1$, $b/a = 1.1$, $c_1/a = 3.0$, $c_2/a = 8.0$).

Fig. 5 illustrates the angular distribution of the SEDFs around the circular cavity with parameters: $ka = 0.1$, $b/a = 1.1$, $c_1/a = 3.0$ and $c_2/a = 8.0$. It can be seen that due to the effect of the upper boundary, the maximum strain energy density has a trend of shifting towards the illuminated side of the cavity. The greater the incident wave number, the greater the effect of the upper boundary on the distribution of SEDFs around the cavity is. One can also see that the SEDFs near the upper boundary are less than those near the lower and the strain energy density at the position of $\theta = 0$ and π becomes great in this case.

The SEDFs at the position of $\theta = \pi/2$ as a function of the distance ratio b/a with parameters: $\beta = 0.1$, $\theta = \pi/2$, $c_1/a = 8.0$ and $c_2/a = 8.0$ are presented in Fig. 6. It can be seen that when the value of b/a is small, the strain energy density decreases with increasing wave number. However, if the value of b/a is greater than a certain number, the strain energy density increases with increasing wave number.

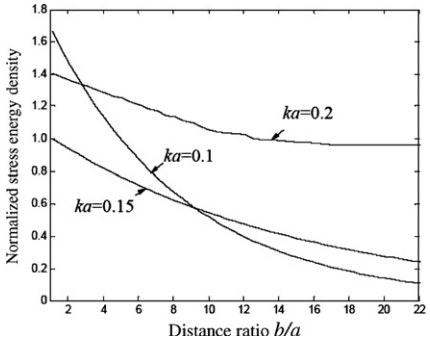

Fig. 6. Normalized strain energy density factor as a function of b/a($\beta a = 0.1$, $\theta = \pi/2$, $c_1/a = 8.0$, $c_2/a = 8.0$).

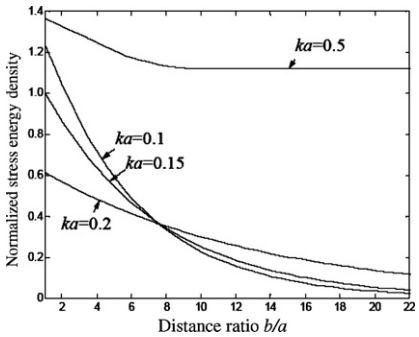

Fig. 7. Normalized strain energy density factor as a function of b/a($\beta a = 0.1$, $\theta = \pi/2$, $c_1/a = 3.0$, $c_2/a = 8.0$).

The SEDFs at the position of $\theta = \pi/2$ as a function of the distance ratio b/a with parameters: $\beta a = 0.1$, $\theta = \pi/2$, $c_1/a = 3.0$ and $c_2/a = 8.0$ are illustrated in Fig. 7. It can be seen that the SEDF first decreases with the distance ratio b/a, and then tends to be invariable as b/a further increases. If the dimensionless wave number is greater than a certain number and the cavity is enough far away from the semi-infinite edge, the strain energy density shows no variation as the distance ratio b/a changes. In contrast to Fig. 6, one can see that the effect of the value of c_1/a in the region of high frequency (great wave number) is greater than that in the region of low frequency. As the value of b/a decreases, the effect of c_1/a on the SEDFs increases.

The SEDFs at the position of $\theta = \pi/2$ as a function of the dimensionless wave number ka with parameters: $\beta a = -0.1$, $\theta = \pi/2$ and $b/a = 1.1$ are presented in Fig. 8. It can be seen that the SEDFs first decrease with dimensionless wave number, then increase and tend to be invariable as ka further increases. Because of the effect of the upper and lower boundaries, the maximum strain energy density deviates from the position of

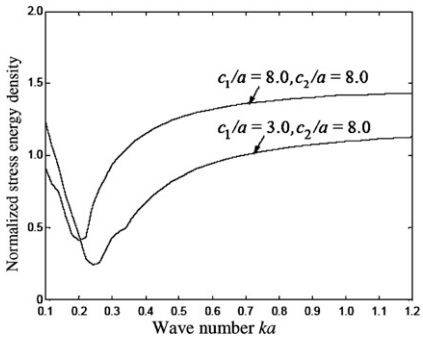

Fig. 8. Normalized strain energy density factor as a function of ka ($\beta a = -0.1$, $\theta = \pi/2$, $b/a = 1.1$).

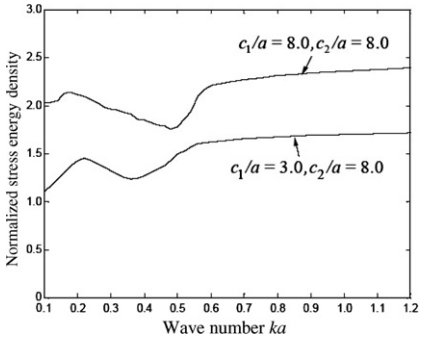

Fig. 9. Normalized strain energy density factor as a function of ka ($\beta a = 0.1$, $\theta = \pi/2$, $b/a = 1.1$).

$\theta = \pi/2$. So when the distance between the center of the cavity and the upper boundary decreases, the strain energy density at the position of $\theta = \pi/2$ decreases.

Fig. 9 shows the SEDFs at the position of $\theta = \pi/2$ as a function of the dimensionless wave number ka with parameters: $\beta a = 0.1$, $\theta = \pi/2$ and $b/a = 1.1$. It can be seen that when the dimensionless wave number is small, the variation of c_1/a has great effect on the SEDFs at $\theta = \pi/2$. In contrast to Fig. 8, one can see that if the non-homogeneous parameter is greater than zero, the effect of c_1/a on the SEDFs at $\theta = \pi/2$ is greater.

6. Conclusion

In the present paper, the strain energy density factors around a circular cavity in a semi-infinite slab of functionally graded materials under anti-plane shear waves are analyzed by employing image method and wave function expansion method. The case that the cavity is free of traction is investigated. The S-theory (Sih, 1973) is applied to determine the potential failure sites around the cavity. The analytical solution and numerical solution of the strain energy density factors around the cavity are presented and analyzed.

In contrast to the homogeneous medium, it is found that the non-homogeneous parameter of materials has great effect on the values and distribution of the SEDFs around the cavity when the values of b/a, c_1/a and c_2/a are small. The maximum strain energy density around the circular cavity increases with increasing non-homogeneous parameter and the incident wave number. When the values of b/a and c_1/a are small, the distribution of the maximum strain energy density varies greatly, and deviates from the position of $\theta = \pi/2$. The effects of b/a, c_1/a and c_2/a on the angular distribution of the SEDFs around the cavity also increase with increasing non-homogeneous parameter.

Therefore, to avoid the fatigue failures of structures, it is proposed that the non-homogeneous parameter should be less than zero in the x direction in Fig. 1, namely, the shear modulus and density of the semi-infinite functionally graded materials decrease in the x direction. The non-homogeneous parameter should decrease with the increase of the values of b/a, c_1/a and c_2/a. If the values of c_1/a and c_2/a are small, a greater value of b/a should be chosen. When the value of b/a is smaller, the maximum SEDF around the cavity increases greatly with a small increase of the frequency of the impact load. We should choose greater values of b/a, c_1/a and c_2/a when designing the semi-infinite functionally graded materials under higher frequency load.

The analytical solutions presented in this paper may be useful for the dynamical analysis and strength design of structures of FGMs and the analysis of fracture problems in FGMs.

Acknowledgements

The paper is supported by the National Natural Science Foundation of China (Foundation No. 10572045) and the Outstanding Youth Foundation of Hei Longjiang Province of China (Foundation No. JC-9). The authors are grateful to the anonymous reviewers for their constructive comments and suggestions.

References

Aboudi, J., Pindera, M.-J., Amold, S.M., 1999. Higher-order theory for functionally graded materials. Composite Part B–Engineering 30 (8), 777–832.

Bi, X.S., Cheng, J., Chen, X.L., 2003. Moving crack for functionally graded material in an infinite length strip under anti-plane shear. Theoretical and Applied Fracture Mechanics 39 (1), 89–97.

Fan, T., 2003. Foundation of Fracture Theory. Science Press, Beijing.

Fang, X.Q., Hu, C., Du, S.Y., 2006. Strain energy density of a circular cavity buried in semi-infinite functionally graded materials subjected to shear waves. Theoretical and Applied Fracture Mechanics 46 (2), 166–174.

Hayir, A., Bakirtas, I., 2004. A note on plate having a circular cavity excited by plane harmonic SH waves. Journal of Sound and Vibration 271 (2), 241–255.

Klyukin, I.I., 1964. Scattering of flexural waves by antivibrators on a plate. Soviet Physics Acoustics 10 (1), 49–53.

Kuo, H.-Y., Chen, T., 2005. Steady and transient Green's functions for anisotropic conduction in an exponentially graded solid. International Journal of Solids and Structures 42 (4), 1111–1128.

Li, C., Weng, G.J., 2000. Dynamic stress intensity factor of a cylindrical interface crack with a functionally graded interlayer. Mechanics of Materials 33 (6), 325–333.

Nobile, L., Carloni, C., Nobile, M., 2004. Strain energy density prediction of crack initiation and direction in cracked T-beams and pipes. Theoretical and Applied Fracture Mechanics 41, 137–145.

Pao, Y.H., Chao, C.C., 1964. Diffractions of flexural waves by a cavity in an elastic plate. AIAA Journal 2 (11), 2004–2010.

Pao, Y.H., Mow, C.C., 1973. Diffraction of Elastic Waves and Dynamic Stress Concentrations. Crane and Russak, New York.

Rice, J.M., Sadd, M.H., 1984. Propagation and scattering of SH-waves in semi-infinite domains using a time-dependent boundary element method. Journal of Applied Mechanics, ASME 51 (3), 641–645.

Roussseau, C.-E., Tippur, H.V., 2001. Influence of elastic gradient profiles on dynamically loaded functionally graded materials: cracks along the gradient. International Journal of Solids and Structures 38 (44), 7839–7856.

Sih, G.C., 1973. A special theory of crack propagation: methods of analysis and solutions of crack problems. In: Sih, G.C. (Ed.), Mechanics of Fracture I. Noordhoof International Publishing, Leyden.

Sladek, J., Sladek, V., Zhang, C., 2005. A meshless local boundary integral equation method for dynamic anti-plane shear crack problem in functionally graded materials. Engineering Analysis with Boundary Element 29 (4), 334–342.

Tan, M., Meguid, S.A., 1996. Dynamic analysis of cracks perpendicular to biomaterial interfaces using a new singular finite element. Finite Element in Analysis and Design 22 (1), 69–83.

Ueda, S., 2001. The surface crack problem for a layered plate with a functionally graded nonhomogeneous interface. International Journal of Fracture 110 (2), 189–204.